Journal of Applied Polymer Science

Bulk Density of Polymer Solid Granules in Vane Cylinder

Jin Ping Qu,[1,2] Shu Feng Zhai,[1,2] Huan Yu Liu,[1,2] Hui Zhuo Chen,[1,2] Shi Kui Jia,[1,2] Zan Huang,[1,2] Yong Qing Zhao,[1,2] Li Ming Liu[1,2]

[1]National Engineering Research Center of Novel Equipment for Polymer Processing, South China University of Technology, Guangzhou 510641, China

[2]Key Laboratory of Polymer Processing Engineering of Ministry of Education, South China University of Technology, Guangzhou 510641, China

Correspondence to: J. P. Qu (E-mail: jpqu@scut.edu.cn)

ABSTRACT: Polymer granules are conveyed and plasticized using an innovational vane extruder composed of several vane plasticizing and conveying units (VPCUs). This study developed a mathematic model to analyze the bulk density of polymer granules in a VPCU, as well as conducted an experiment to investigate the effects of device geometry, polymer properties, and operating conditions on the model. By comparing the theoretical model data with the experiment data, the proposed model of bulk density is found to be aligned with actual conditions, thus providing a basis for device and process optimization. © 2013 Wiley Periodicals, Inc. J. Appl. Polym. Sci. 130: 842–850, 2013

KEYWORDS: rheology; theory and modeling; extrusion

Received 5 November 2012; accepted 3 March 2013; published online 5 April 2013
DOI: 10.1002/app.39231

INTRODUCTION

Various methods such as extrusion, injection molding, and blow molding are used in polymer processing. Most polymer processing instruments are based on the screw. Polymer processing is generally divided into several steps: solid conveying, melting, supercharging and pumping, mixing, and devolatilization. In the solid-conveying section, the polymer materials are not only being conveyed forward, more importantly, they are being compressed to prepare for plasticizing and melting in the next section. How well the screw design matches the compaction behavior of the resin for a given set of process conditions has significant influence on extruder performance. However, the design of the screw sections is often done on account of the past experience and with little knowledge of the resin compaction behavior. An improved design would ideally include screw performance prediction using variable bulk density.

The phenomenon and effects of the bulk density on polymer processing have been studied by numerous researchers.[1,2] Bulk density is defined as the density of polymeric material, either powders or particles, including the voids between them. Bulk density is one of the significant properties of bulk material. Before the mass flow rate of the process can be calculated, comprehending bulk density and its variation with a certain degree of confidence in the theories[3] of extruder screw design is required. Thus, predicting or estimating the magnitude of bulk density under combined effects is necessary because the compressibility of the bulk material determines, to a large extent, the solid-conveying behavior in polymer processing.

The earliest appropriate mathematical model that described the mechanism of solid conveying was established by Darnell and Mol[4] in 1956, and was based on solid static friction and static equilibrium. In 1969, Schneider[5] obtained a more realistic stress distribution by revising the assumption of isotropic stress distribution in the Darnell-Mol[4] model and by assuming a specific ratio between compressive stress in the down-channel direction and stresses in the other directions. In 1972, Broyer[6,7] and Tadmor[6,7] modified the Darnell-Mol[4] model, and considered the effects of screw helix and temperature variation. The well-known Darnell-Mol[4] model is a one-dimensional plug flow. More recently, other refinements were applied by Chung,[8] Lovegrove,[9] Williams,[10,11] and Zhu and Chen.[12] The plug flow model has provided a basis for many theoretical and experimental investigations of solid conveying in screw extruders.

A number of investigations concerning the rheology of bulk density material have been conducted to close the gap left by the extruder theory. Cheng and Gogos[13] studied bulk density variation in the compaction period and examined the actual area, where pellets are in contact with the metal wall under various pressures. Smith and Parnaby[14] provided the isothermal bulk density data for a number of commercially available

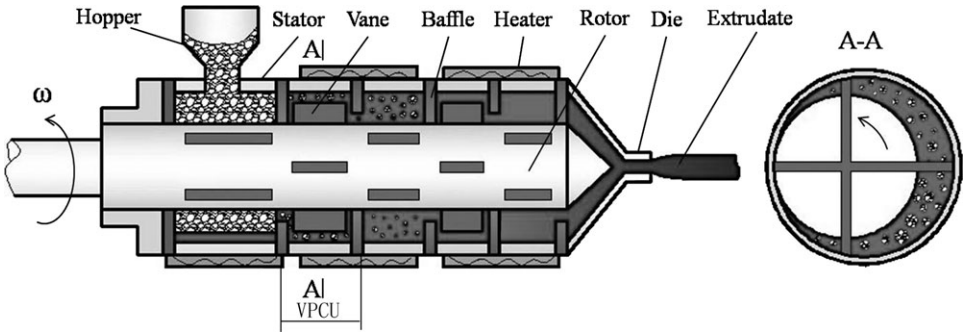

Figure 1. Schematic diagram of the vane extruder.

plastics with practical ranges of uniform hydrostatic pressure, as well as the regression fitted polynomials for each plastic. Potente and Schöppner[15] developed formulas for calculating the bulk density of granules in the extruder screw channel.

This study introduces a novel vane extruder[16,17] in which a complete extrusion system is composed of several vane plasticizing and conveying units (VPCUs), as shown in Figure 1. A group of VPCUs is composed of a stator, an eccentric rotor, four vanes, and two baffles that are used to feed and discharge the material. The four vanes are installed in pairs in the rectangular through hole of the rotor. The conveying mechanism of the vane extruder is based on the vane elongational flow, which is completely different to the screw extruder.

This study constructs a mathematical model of the bulk density in the solid compacting process of a vane extruder based on stress distribution analysis and then provides an analytical solution. The data from the theoretical model of bulk density are then compared with the physical formula data. The theoretical model results show that the bulk density in the compacting process of polymer solids in the vane extruder is affected by device geometry, polymer properties, and operating conditions.

THEORETICAL MODEL

The vane extruder is a novel extruder that differs from an ordinary extruder. The schematic diagram of the solid-conveying zone in the vane extruder is shown in Figure 2. The mathematical model is established by using a cylindrical coordinate system to describe the movement of the solid pellets in the chamber.

Various forces acting on the micro-element are illustrated in Figure 3. These forces can be expressed in terms of coefficients of friction, local geometry, and the differential pressure increment, which compensate for other forces.[18]

Our previous study[19] indicated that the variation of pressure applied by the rear vane could be expressed as follows:

$$P_1 = \frac{1}{2}P_1(\theta_v)\left(1+\exp\left\{\frac{K_z f_b\left(r_2+r_1-\frac{d^2}{4r_2}\right)(r_2{}^2-r_1{}^2+2K_r(f_s-f_r)Br_1{}^2-2K_r f_s B(r_2{}^2-r_1{}^2)}{K_\theta B(r_2{}^2-r_1{}^2)}\frac{\pi}{2}+\right.\right.$$
$$\left.\left.\frac{K_z f_b d}{K_\theta B}\left[\sin\theta_v-\sin(\theta_v+\frac{\pi}{2})\right]+\frac{K_z f_b d^2}{8K_\theta B r_2}[\sin 2\theta_v-\sin(2\theta_v+\pi)]\right\}\right) \quad (1)$$

where θ_v is the angular coordinate of the rear vane of VPCU in the cylindrical coordinate system, and $P_1(\theta_v)$ is the pressure on the rear vane.

$$\text{Supposing } c_p = \frac{P_1(\theta_v+\frac{\pi}{2})}{P_1(\theta_v)} \quad (2)$$

$$\mathrm{P} = \frac{P_1(\theta_v+\frac{\pi}{2})+P_1(\theta_v)}{2} \quad (3)$$

The following expression of P is obtained by substituting eq. (2) into eq. (3):

$$P = \frac{(1+c_p)}{2}P_1(\theta_v) \quad (4)$$

where P is the pressure acting on the whole granular system in one chamber.

The experimental work of Chung[8] indicated that the variation of material density could be expressed by the following semi-empirical equations:

$$\rho = \rho_{\max} - (\rho_{\max}-\rho_{\min})\cdot \mathrm{e}^{-c_0 P} \quad (5)$$

$$c_0 = b_0 + b_1 * T + b_2 * T^2 + b_3/(T_g - T) \quad (6)$$

where $\rho_{\max}$ is the maximum bulk density at infinitely high pressure which is assumed as the solid-phase density of the material in this article; $\rho_{\min}$ is the minimum bulk density at zero pressure, which is assumed as the bulk density at angle α; and ρ is the actual density of the material. c_0 is the bulk density pressure

Applied Polymer SCIENCE

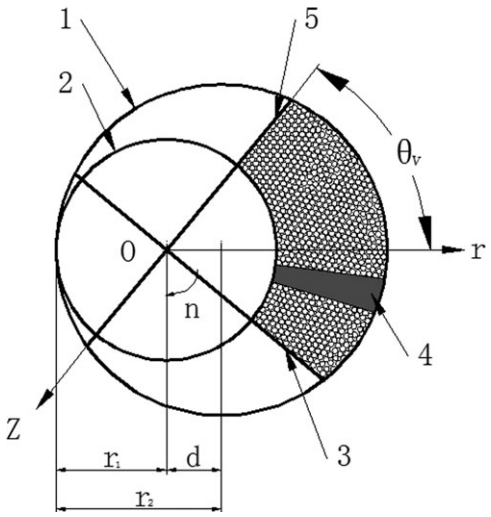

Figure 2. Schematic diagram of the solids conveying zone: (1) stator, (2) rotor, (3) front vane, (4) differential element and (5) rear vane.

coefficient function. b_0,b_1,b_2, and b_3 are the coefficient parameters of c_0. T and T_g are the processing temperature and the glass transition temperature of the material, respectively. B is the axial width of the VPCU.

The torque exerted on the rotor shaft is expressed as follows.

$$M = P_1(\theta_v)[r(\theta_v) - r_1]Br(\theta_v) - P_1(\theta_v + \frac{\pi}{2})\left[r\left(\theta_v + \frac{\pi}{2}\right) - r_1\right]B_r\left(\theta_v + \frac{\pi}{2}\right) \quad (7)$$

The following expression of ρ is obtained by substituting eq. (2), (3) and (7) into eq. (5):

$$\rho = \rho_{\max} - (\rho_{\max} - \rho_{\min}) \exp\left\{\frac{\frac{(1+c_p)}{2}c_0 M}{B[r(\theta_v) - r_1]r(\theta_v) - Bc_p\left[r\left(\theta_v + \frac{\pi}{2}\right) - r_1\right]r\left(\theta_v + \frac{\pi}{2}\right)}\right\} \quad (8)$$

According to (8), the bulk density expression in the chamber during the compacting and conveying of polymer solids is obtained as a function of ψ, which is defined as $\psi = (\frac{1}{4})\pi - \theta_v$, indicating that the bulk density can be derived from the total torque M of the rotor. Therefore, the bulk density in the first VPCU can be studied by measuring the total torque M of the rotor.

EXPERIMENTAL

Material

The characteristics of the materials used to prepare the experiment are provided in Table I.

Experimental Device

A visual experimental device is designed to study the solid-conveying and compaction mechanism of the vane extruder, as shown in Figure 4. The equipment consists of the driving and compaction systems. When the rotor is rotating, the torque sensor can measure the total torque of the rotor. The compaction system comprises one group of VPCUs, and the eccentricity d between the rotor and the stator can be adjusted from 0 mm to 3 mm. To observe the compaction process, the baffle of a VPCU is made of quartz glass, and the discharge port is along the circumferential direction of the rotor. The experimental phenomena can be observed through the visualization window. This equipment has three stators with different angles of discharge port β (30°, 35°, and 40°), which can be accordingly installed to study the effects of different discharge ports on bulk density. The length (L) of vane is 35 mm, and the diameter (D) of the rotor in the device is 40 mm. The chamber has the largest volume when the angle $\theta_v = (1/4)\ \pi$.

Experimental Program

Given that the motions of the four cavities were the same, one material-filled cavity was chosen for the experiments. A number of factors affected bulk density, including of device geometry (eccentricity and discharge port), polymer properties (phase morphology, frictional coefficient, and material shape), and operating conditions (temperature and rotating speed). In each experiment, one variable was varied under the same conditions. The experimental programs had seven variables (material shape, phase morphology, eccentricity, discharge port, friction coefficient, rotating speed, and temperature), as shown in Table II. In Experiment #1, the variable was the shape of the material. In Experiment #2, the variable was the different materials with different phase morphologies: PP, ABS, PVC, and HIPS. In Experiment #3, the variable was eccentricity, which ranged from 1 mm to 3 mm. In Experiment #4, the variable was the discharge port, which varied from 30° to 40°. The variable in Experiment #5 was friction coefficient. Rotating speed, which varied from 2r/min to 20r/min, was the variable in Experiment #6. In Experiment #7, the variable was the temperature, which ranged from 30°C to 120°C. In Experiment #8, the parameters of the experiment were the following: 2r/min rotating speed, 80°C temperature, 3 mm eccentricity, and 40° discharging angle. Before the start of each experiment, filling the cavity with material up to its maximum volume was necessary. The experiments then ensued, and the total torque of the rotor was recorded. Finally, based on eq. (8), the bulk density was obtained as a function of the angle.

RESULTS AND DISCUSSION

Figure 5 shows the comparison between the theoretical model bulk densities of ABS material at various temperatures and the physical formula data. The physical formula used in the study is

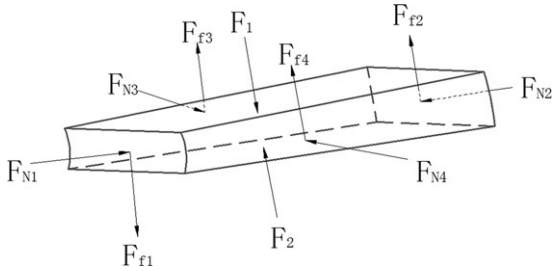

Figure 3. Forces acting on the differential element along the circumferential direction.

Table I. Characteristics of the Materials

Materials	Supplier	Characteristics
Polypropylene (PP)(CJS-700)	Petrochem. Co., China	ρ_m 920 kg/m^3
Linear low density polyethylene (LLDPE)(DFDA-7042)	Petrochem. Co., China	ρ_m 930 kg/m^3
Acrylonitrile butadiene styrene copolymers (ABS)(9555)	Dow chemical corporation	ρ_m 1060kg/m^3
High impact polystyrene (HIPS)(GH660)	Petrochem. Co., China	ρ_m 1035kg/m^3
Polyvinylchloride (PVC)(S-700)	Petrochem. Co., China	ρ_m 1040kg/m^3
Epoxidized soybean oil (ESO)(X-20)	Petrochem. Co., China	-

$\rho = \frac{m}{v}$. In the theoretical model data, the parameters are as follows: $b_0 = -0.65 \times 10^{-7}$MPa^{-1}, $b_1 = -0.1 \times 10^{-8}$ (MPa^{-1}°C^{-1}), $b_2 = 0$, and $b_3 = -0.54 \times 10^{-6}$°C/MPa, $d = 3$ mm, $D = 40$ mm, and $L = 35$ mm. Figure 5 clearly shows that the theoretical model data and the physical formula data have the same trends, and the curves are relatively matched, particularly with small angle ψ. According to this trend, the solid compaction process is divided into the particle re-arrangement period ($\psi < 0.3$ rad) and the compaction period ($\psi > 0.3$ rad). In the particle re-arrangement period, the bulk density is low and increases slowly with the rotating angle of the rotor. In this period, the solid material are loosely stacked in the cavity, and numerous voids exist between the material. Solid particle movement is merely a spatial re-arrangement of the material that facilitates a slow increase in bulk density. During the compaction period, the elastic deformation of the material first occurs near the point of high stress, thus resulting in a sharp rise in bulk density. Upon further compression, plastic deformation of the solid particles occurs, and some particles rupture. Under this condition, although the bulk density increases, the theoretical model data are smaller than the physical formula data. A small gap exists between the top of the vane and the inner surface of the stator. When the volume constituted by the stator, the rotor, two adjacent vanes, and the baffles decreases, that is, the materials are compacting, a small portion of the materials will be squeezed out through the gap from one cavity to another. However, in the physical formula $\rho = \frac{m}{v}$, v is decreasing, and m is constant, such that the theoretical model data is smaller than the physical formula data. Finally, the solid materials are completely compacted. Thus, the particle re-arrangement period is the no-deformation stage, whereas the compaction period is the elastic and plastic-deformation stage.

The final theoretical model bulk density is significantly lower than the physical formula data. The obvious difference in final bulk density between the theoretical model and the physical formula data may be attributed to discharging. When the materials begin to be discharged, the volume of the chamber is relatively small .The materials are compacted to the maximum limit in the VPCU. Thus, the bulk density exhibits minor changes. With the physical formula data, the quantity m is constant, and the volume is decreasing, thus resulting in a steep increase in the physical formula bulk density. On this account, the final theoretical model bulk density is significantly lower than the physical formula data.

As shown in Figure 6, the compaction process comprises charging, compacting, and discharging. Unlike the physical formula, bulk density data increase linearly. The theoretical model bulk density evidently differs from the physical formula data in terms of leakage and discharging. Thus the theoretical model is more suitable for reflecting the variations of the bulk density in the vane extruder.

Polymer Property

In Experiment #1, the effects of the material shape on bulk density were studied. Figure 7, which was obtained from the

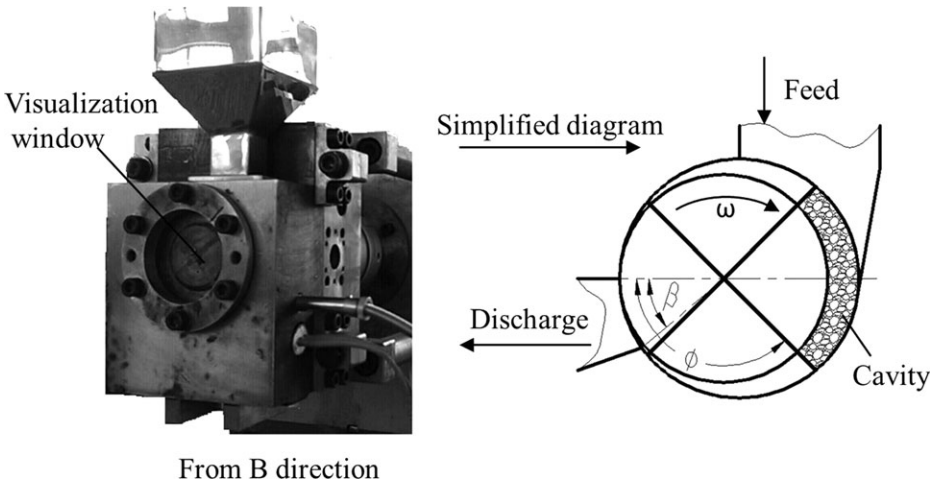

Figure 4. Schematic diagram of visual experimental device.

Table II. Experimental Programs

	Material	Phase morphology	Eccentricity (mm)	Discharge (°)	Rotating speed (r/min)	Temperature (°C)
#1	LLDPE(powder)	Crystalline	3	40	2	80
	LLDPE(pellet)					
#2	PP(powder)	Crystalline	3	40	2	120
	ABS,PVC,HIPS (powder)	Amorphous				
#3	LLDPE(powder)	Crystalline	1			
			2	40	2	80
			3			
#4	LLDPE (powder)	Crystalline		30		
			3	35	2	80
				40		
#5	LLDPE (powder)	Crystalline	3	40	2	80
	LLDPE(ESO) (powder)					
					2	
					5	
#6	LLDPE(powder)	Crystalline	3	40		80
					10	
					20	
						30
						50
#7	ABS(powder)	Amorphous	3	40	2	
						90
						120
#8	LLDPE(pellet)	Crystalline	3	40	2	80

theoretical model, clearly shows that, the powder and the pellet of LLDPE exhibit similar behavior, and that the bulk density of the LLDPE increases with the rotating angle of the rotor. When the angle is relatively small, the change in the bulk density is minimal. With the rotating angle of the rotor, the slope of the curve describing the relationship between the bulk density and the angle increases. As shown in the compaction process (Figure 6), the rotating of the rotor facilitates a decrease in the volume of the cavity as well as the rearrangement of particles. After the rearrangement of the particles, the voids between the material are filled. The surfaces of particles are in contact with one another in the compressional deformation field, which results in a steep increase in bulk density. The negligible differences in bulk density between the powders and the pellet denote that the shape of material has a minor effect upon the bulk density of the material, which is different from the screw extruder. This finding also denotes that the vane extruder has a more effective adaptability to the material.

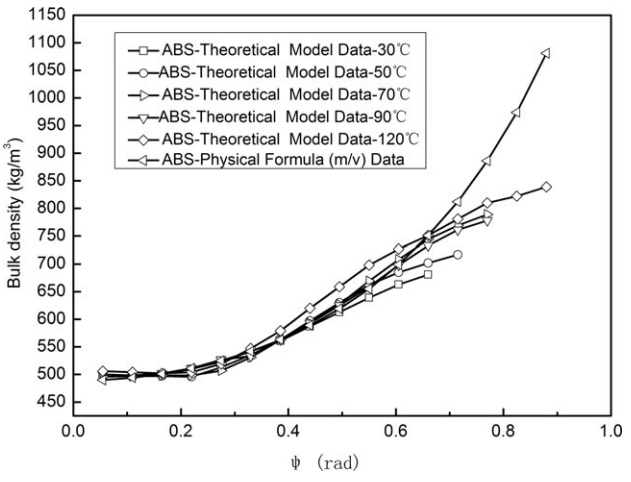

Figure 5. Comparison between the theoretical model bulk density and the physical formula data.

Experiment #2 compared the bulk density between the crystalline material (PP) and the amorphous materials (ABS, PVC, and HIPS) at the given temperature (120°C). The data are obtained by using the theoretical model. The compaction progress in Figure 6 clearly shows that, while the rotor is rotating, the void volume between the particulate solids decreases and the particles are deformed and even fractured, resulting in an increase in bulk density. Figure 8 also clearly shows that in the initial period, the different polymer materials have very similar bulk density. However, differences in the bulk density for different polymer materials gradually increase with the rotating angle of the rotor. The bulk density of the amorphous (PVC) material is significantly higher than that of the amorphous (ABS)

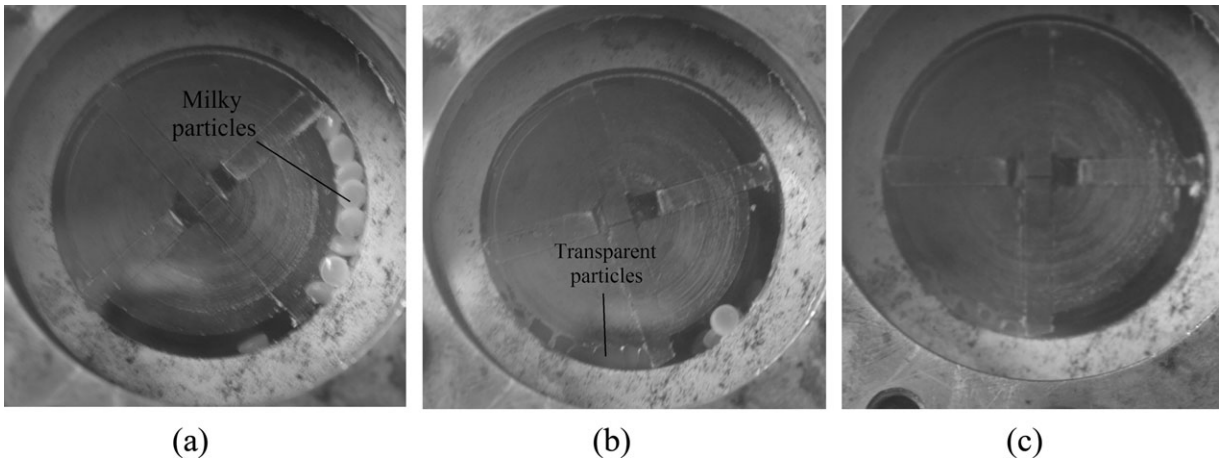

Figure 6. Photograph of compaction process of materials LLDPE at 80°C in the visual experimental device.

material, particularly in the period of $\psi > 0.5$ rad. This result may be attributed to the various material properties that can affect the solid compaction process, such as glass transition temperature T_g. Hyun and Spalding[2] suggested that amorphous polymers with low T_g, such as PVC, are easily compacted. Under the same experimental conditions, T_g of the PVC is lower than that of ABS. Therefore, the bulk density of PVC is higher than that of ABS.

Device Geometry

The rotor eccentricity of the inner stator is one of the innovations in the vane extruder. The quantity of material that can fill the chamber increases as eccentricity increases. In Experiment #3, the quantity of LLDPE held in the chamber when completely full were 2.8, 3.2, and 3.5 g, when the eccentricities were 1, 2 and 3 mm respectively. Figure 9 clearly shows that when the chamber is completely filled with material, significant differences are observed between the initial and final bulk densities. The initial bulk density decreases when eccentricity increases, whereas the final bulk density increases when eccentricity increases. Calculating from the schematic diagram of the solid conveying (Figure 2), the maximum cavity $v_{max} = B\left[\frac{\pi}{4}(r_2{}^2 - r_1{}^2) + \sqrt{2}r_2 d + \frac{1}{2}d^2\right]$, the minimum cavity $v_{min} = B\left[\frac{\pi}{4}(r_2{}^2 - r_1{}^2) - \sqrt{2}r_2 d - \frac{1}{2}d^2\right]$, and the volume of the maximum cavity increases with the eccentricity d. However, the volume of the minimum cavity decreases with the eccentricity d. When $\psi < 0.1$, the cavity approaches the maximum volume. A lager eccentricity implies a lager v_{max} and a loose arrangement of granules, which results in a decrease in bulk density as the eccentricity increases. However, with the rotating of the rotor, the materials are compacted as shown in Figure 6. The volume of the cavity decreases, particularly in the final stage of compaction. A larger eccentricity implies a smaller volume of the cavity and greater quantity of material in the cavity. Thus, the voids between the granules are completely filled in the final stage of compaction. Moreover, a larger eccentricity results in larger bulk density. The differences of bulk density at different eccentricities show that a larger eccentricity is necessary for the

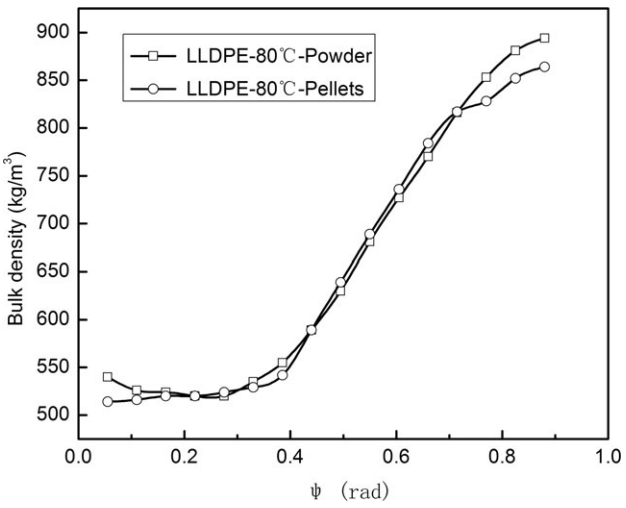

Figure 7. Comparison of bulk densities of polymer materials with different material shapes.

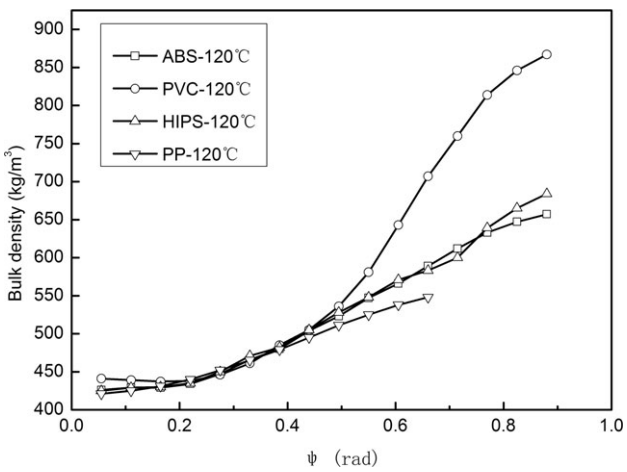

Figure 8. Comparison of bulk density of polymer materials with different phase morphology.

Applied Polymer SCIENCE

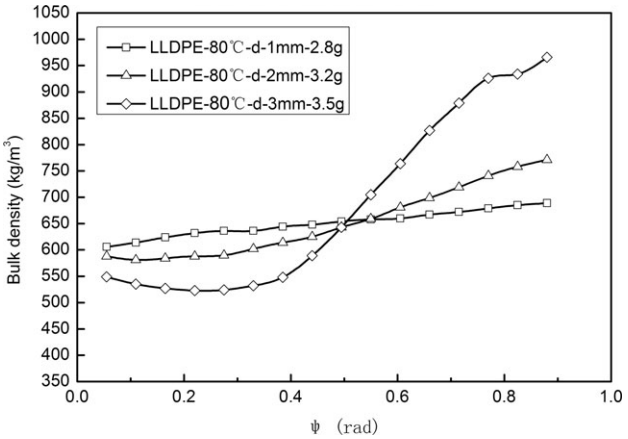

Figure 9. Comparison of bulk density of polymer materials in different eccentricity.

compaction of the material in the solid-conveying zone of the vane extruder.

In the vane extruder, the size and location of the discharge port in the first VPCU are crucial for the bulk density. In Experiment #4, three different discharge ports were used to study their effects. The angles of three discharge ports with smooth inner surface were 30°, 35°, and 40°. The three curves at 30°, 35°, and 40° indicate that the bulk density steeply increases with the rotating of the rotor, and that a larger discharge port makes bulk density smaller, as shown in Figure 10. The data were obtained from the theoretical model. In the vane extruder, the discharge direction is along the axial direction of the rotor, which is in contrast to the visual experimental device where the discharge direction is along the circumferential direction of the rotor. However, the discharge port on the baffle can also be designed according to this experiment. The discharge port on the baffle should be larger than the limiting angle $\theta v = [4\rho_{\min}\alpha + (\rho_{\min} - \rho_{\max})\pi]/4\rho_{\max}$, where the solid materials are compacted to the maximum. Otherwise, the vanes will be damaged. The discharge port should not be too large so that the bulk density can be established and the material can be compacted.

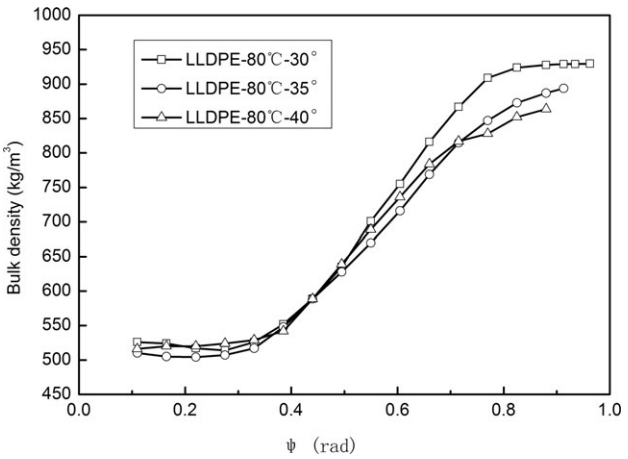

Figure 10. Comparison of bulk density of polymer materials in different discharge position.

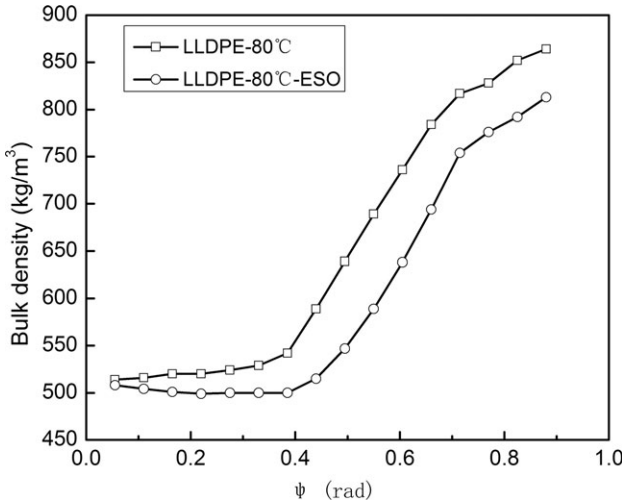

Figure 11. Comparison of bulk density of polymer materials with and without epoxy soybean oil (ESO).

Figure 11 clearly shows that the curves of bulk density with and without epoxy soybean oil (ESO) have the same trend. However, the bulk density of LLDPE with ESO is lower than the bulk density of LLDPE without ESO. With the rotating angle of the rotor, the volume of the chamber decreases and the materials are compacted, which induces the bulk density to increase. The solid particle conveying of the screw extruder is established on the basis of frictional drag, and the heat caused by the friction has a significant effect on solid melting and polymer processing. However, in the vane extruder, materials are forcibly conveyed owing to the periodic change of chamber with the rotating angle of the rotor. Thus, the fiction coefficient has negligible effect on the solid-conveying in the vane extruder and the vane extruder has an improved adaptability to the material.

Operation Condition

Experiment #6 studied the effects of the rotating speed on the bulk density. The results obtained from the theoretical model, as shown in Figure 12, demonstrate that the whole bulk density of LLDPE increases with the rotation of the rotor, whether at

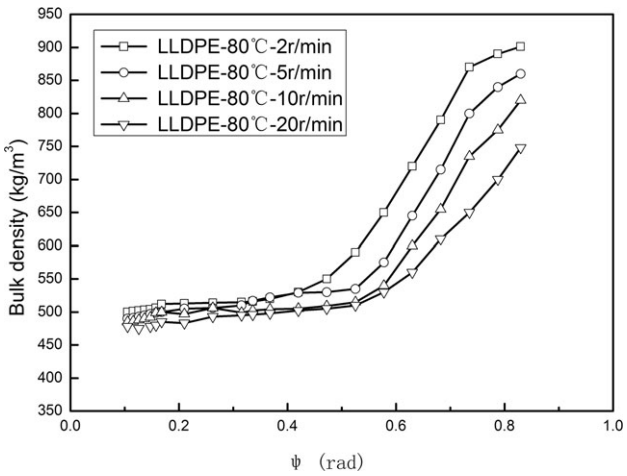

Figure 12. Comparison of the bulk density of polymer materials in different rotational speed.

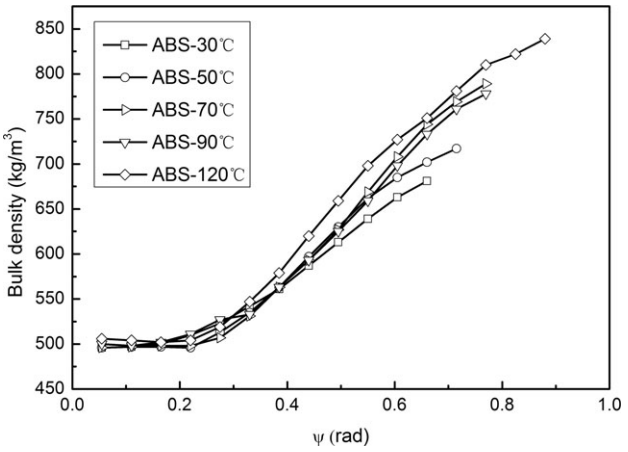

Figure 13. Comparison of bulk density of polymer materials in different processing temperature.

high or low rotational speeds. Figure 12 also clearly shows that in the final stage of compaction, bulk density decreases as rotational speed increases, that is, the bulk density at high rotating speed is lower than that at low rotating speed. As shown in Figure 6, at high rotating speed, the rotor quickly shifts from one angle to another, and the materials are quickly discharged from the VPCU. Thus, the materials have little time to be compacted. As a result, at the final stage of compaction, the bulk density is lower at high rotating speed than at low rotating speed. Figure 12 also shows that the initial bulk density of the LLDPE has minimal effect on the rotation of the rotor. During the initial period, the materials do not completely fill the chamber and cling closely to the front vane. Given the rotation angle of the rotor, the materials move to the middle area, such that neither the front nor the latter vanes can compact the material, which results in a minimal variation of bulk density. The results indicate that higher rotating speed has a negative effect on the compaction process. Thus, the polymer obtained at lower rotating speeds has higher bulk density than that obtained in higher rotating speeds.

Experiment #7 investigated the effects of temperature on bulk density. The results obtained from the theoretical model, shown in Figure 13, clearly shows that the variations of bulk density are not significantly different at various temperatures. The curves show the same trend of the bulk density of solid granules increasing with the rotation angle of the rotor. After an initial slow rise, the rate of increase of the bulk density at a relative high temperature rapidly rises, particularly at 120°C. This phenomenon can be attributed to the various material properties that can affect the solid compaction process, such as glass transition temperature T_g. The glass transition temperature T_g of ABS is about 100°C, and when the temperature exceeds the glass transition temperature, the macromolecules can move freely, allowing the polymer material to be easily compacted by external forces. As a result, bulk density increases steeply. Based on this experiment and the actual process, the temperature setting of the feeding section should be high enough to properly compact the material.

Temperature has a significant effect on the compressibility coefficient function c_0, which increases rapidly with temperature. According to the experimental data, the compressibility coefficient function c_0 of the ABS material in the vane extruder is

$$c_0 = -0.65 \times 10^{-7} + 0.1 \times 10^{-8} * T - 0.54 \times 10^{-6}/(T_g - T) \quad (9)$$

Equations (6) and (9) yield $b_0 = -0.65 \times 10^{-7}\text{MPa}^{-1}$, $b_1 = -0.1 \times 10^{-8}$ ($\text{MPa}^{-1}{}^{\circ}\text{C}^{-1}$), $b_2 = 0$, and $b_3 = -0.54 \times 10^{-6}{}^{\circ}\text{C}$/MPa in the vane extruder.

CONCLUSIONS

The bulk density in the solid-conveying section of the vane extruder was analyzed using a convergent wedge slot model, and the analytical solution of the bulk density was obtained using a semi-empirical equation $\rho = \rho_{\max} - (\rho_{\max} - \rho_{\min}) \cdot e^{-c_0 P}$. The theoretical model data of the bulk density was compared with the physical formula $\rho = \frac{m}{v}$ data.

The theoretical model results show the effects of polymer properties, device geometry, and operating conditions on bulk density during the compaction of polymer solids in the vane extruder. The following conclusions were drawn: (1) During the initial stage of compaction, the polymer powder and pellets can nearly reach the same bulk density. However, during the final stage of compaction, the powder can reach a higher bulk density than the pellets. (2) The bulk density of amorphous materials is closely related to glass transition temperature T_g, such that a higher T_g results in higher bulk density. (3) A greater eccentricity results in more significant changes in bulk density (smaller initial bulk density but higher final bulk density). (4) Later discharging can result in higher bulk density. (5) The addition of epoxy soybean oil (ESO) reduces the friction coefficient, which results in smaller bulk density. (6) Higher rotating speed has a negative effect on the compaction process, which results in lower bulk density. (7) A higher processing temperature is beneficial to the compaction of material and can result in higher bulk density.

ACKNOWLEDGMENTS

The authors wish to acknowledge the Fundamental Research Funds for the Central Universities (NO. 2011ZM0063), the National Nature Science Foundation of China (Grants 10872071, 50973035, and 50903033) , the National Key Technology R&D Program of China (Grants 2009BAI84B05 and 2009BAI84B06) and the National Natural Science Foundation of China-Guangdong Joint Foundation Project (U1201242) for their financial support.

NOMENCLATURE

r_2	Radius of the stator(m)
d	Eccentricity between baffles and materials
ψ	Absolute angle of the materials micro-unit in the closed volume (rad)
ρ	Actual bulk density of the materials (kg/m^3)
T_g	Glass transition temperature of the materials (°C)

T	Processing temperature (°C)
C_0	Bulk density pressure coefficient function (MPa^{-1})
b_0, b_1, b_2, b_3	Coefficient parameters of C_0
F_{N1}	Radial force exerted by the rotor (N)
F_{N2}	Radical force exerted by the stator (N)
$F1$	Circumferential pressure at θ
$F2$	Circumferential pressure at $\theta + d\theta$
F_{f1}	Frictional force on the rotor surface
F_{N3}	Circumferential force to promote the differential element (N)
F_{N4}	Circumferential force to retard the differential element (N)
F_{f3}	Friction forces on the front baffle surface(N)
F_{f4}	Friction forces on the rear baffle surface(N)
K_r	Radical pressure coefficient
K_θ	Circumferential pressure coefficient
K_z	Axial pressure coefficient
f_s	Friction coefficient between the rotor and the materials
f_r	Friction coefficient between the stator and the materials
f_b	Friction coefficient between the baffle and the materials
P	Pressure on the whole granules system (MPa)
f_p	Coefficient of pressure transmission
M	Quantity of the materials (kg)
V	Volume of the closed volume
$P_1(\theta_v$	Pressure on the rear vane (MPa)
M	Torque on the rotor shaft (N m)
A	Position angle of the discharge port

REFERENCES

1. Qiu, D. Q.; Prentice, P. *Polym. Technol.*, **1998**, *17*, 23.
2. Hyun, K. S.; Spalding, M. A. *Polym. Eng. Sci.* **1990**, *30*, 571.
3. Chung, C. I.; Hennessary, W. J.; Tusim, M. H. *SPE J.* **1977**, *17*, 9.
4. Darnell, W. H.; Mol, E. A. J. *SPE J.* **1956**, *12*, 20.
5. Schneider, K. Institute of Plastics Processing (IKV), Aachen, **1969**.
6. Broyer, E.; Tadmor, Z. *Polym. Eng. Sci.* **1972**, *12*, 12.
7. Tadmor, Z.; Broyer, E. *Polym. Eng. Sci.* **1972**, *12*, 378.
8. Chung, C. I. *Polym. Eng. Sci.* **1975**, *15*, 29.
9. Lovegrove, J. G. A.; Williams, J. G. *J. Mech. Eng Sci.* **1973**, *15*, 195.
10. Lovegrove, J. G. A.; Williams, J. G. *J. Mech. Eng. Sci.* **1973**, *15*, 114.
11. Lovegrove, J. G. A.; Williams, J. G. *Polym. Eng. Sci.* **1974**, *14*, 589.
12. Zhu, F.; Chen, L. *Polym. Eng. Sci.* **1991**, *31*, 1113.
13. Cheng, C. Y.; Gogos, C. G. 37th SPE ANTEC, New Orleans, LA, **1979**, p.156.
13. Qiu, D. Q.; Prentice, P. *Polym.Tech.* **1998**, *17*, 23.
14. Smith, N. M.; Parnaby, J. *Polym. Eng. Sci.* **1980**, *20*, 830.
15. Potente, H.; Schöppner, V. *Int. Polym. Proc.* **1995**, *10*, 289.
16. Qu, J. P. China Patent, 200810026054.X (**2008**).
17. Qu, J. P.; Chen, H. Z.; Liu, S. R.; Liu, L. M.; Yin, X. C.; Liu. Q. J.; Guo, R. B. *J. Appl. Polym. Sci*, **2012**,DOI: 10.1002/app.38573.
18. Tadmor, Z.; Gogos, C. G. Polymer Rheology and Non-Newtonian Fluid Mechanics, 2nd ed.; Wiley: New Jersey, **2006**; p 484.
19. Qu, J. P.; Zhao, X. Q.; Li, J. B.; Cai, S. Q. *J. Appl. Polym. Sci.*, **2012**,DOI: 10.1002/app.36806.